JMEPEG (1998) 7:205-213

The Effect of Zr on the Low-Cycle Fatigue Behavior of NiAl at 1000 K

B.A. Lerch, R.D. Noebe, and K.B.S. Rao

(Submitted 14 April 1995; in revised form 21 November 1997)

The effect of a 0.1 at.% alloying addition of Zr on the low-cycle fatigue behavior of polycrystalline NiAl was determined at 1000 K and compared to that of binary NiAl. Samples of binary NiAl and the Zr-doped alloy were processed by either HIP consolidation or extrusion of prealloyed intermetallic powders. The cyclic stress response, cyclic stress-strain behavior, and strain-life relationships were all significantly influenced by the microalloying addition of Zr, regardless of the processing technique. A detailed examination of the post-tested low-cycle fatigue (LCF) samples was conducted by optical and electron microscopy to determine variations in fracture and deformation modes and to characterize any microstructural changes that occurred during LCF testing. Differences in LCF behavior due to the Zr addition are attributed to the strong effect that Zr has on modifying the deformation behavior of the intermetallic.

Keywords damage, deformation, intermetallic, low cycle fatigue, NiAl

1. Introduction

The substantial research that has been performed on binary NiAl has shown that this ordered intermetallic is deficient as a structural material in two areas: low temperature ductility and high temperature strength (Ref 1, 2). Therefore, any useful structural alloy based on NiAl will at the minimum contain microalloying additions to alter or enhance these critical properties (Ref 3, 4). The effects of microalloying additions on properties range significantly. Some microalloying (<1 at.%) additions such as Fe and Ga can have a mildly beneficial effect on the tensile ductility of NiAl single crystals (Ref 5) but have essentially no impact on the properties of polycrystalline alloys (Ref 6). Most other microalloying additions, including B and Cr, adversely effect low temperature tensile ductility and increase the brittle-to-ductile transition temperature (BDTT) (Ref 7-9). A few additions, such as Ta, Hf, Nb, Zr, and Ti, while not beneficial to low temperature properties, can have a very significant strengthening effect at elevated temperatures (Ref 10-12). Of these elements, Zr is the one microalloying addition that has been studied in the most detail due to its extremely dramatic impact on the overall behavior of NiAl.

Zirconium additions to NiAl were first studied by Barrett (Ref 13) as a method for enhancing the cyclic oxidation resistance of the aluminide. The presence of Zr increased the cyclic oxidation resistance of NiAl by up to several orders of magnitude depending on temperature by reducing the amount of oxide spalled during the cooling cycles (Ref 13). The optimum level for cyclic oxidation resistance was determined to be approximately 0.1 at.% with a significant loss in oxidation resistance observed at greater Zr levels due to internal oxidation (Ref 14). Subsequently, the effect of minor (0.05 to 0.1 at.%) Zr additions on the tensile and compression properties of NiAl (Ref 6, 15, 16) was studied. Results were equally dramatic though not necessarily positive. Zirconium additions decreased the already poor room temperature tensile ductility of polycrystalline NiAl and significantly increased (by up to a factor of two) the BDTT. The increase in BDTT was attributed to the segregation of Zr to the grain boundaries (Ref 17) and the subsequent inhibition of localized deformation mechanisms (Ref 18). In addition, these deformation studies also indicated that some Zr was distributed within the alloy in solid solution and acted as an extremely potent solid-solution strengthening agent. This led to a detailed study of the high temperature deformation behavior of NiAl(Zr) alloys (Ref 19). The results were again dramatic, with even the smallest Zr additions (0.05 to 0.1 at.%) resulting in alloys that were several times stronger than binary NiAl under identical conditions of temperature and imposed strain rate. Balancing both creep strength considerations and environmental observations, Whittenberger and Noebe (Ref 19) concluded that the optimum level of Zr in NiAl was between 0.1 and 0.3 at.%. Another interesting aspect of this work was that Zr appeared to alter the bulk deformation behavior of NiAl from a dislocation climb controlled process in the undoped alloy to one that was dominated by a viscous glide creep mechanism in the Zr-doped material. Therefore, Zr appears to modify both the localized (Ref 18) and bulk deformation processes (Ref 19) in NiAl.

The effect of Zr on the cyclic deformation behavior of NiAl has not been previously investigated. The studies already described would indicate that Zr could have both beneficial and detrimental effects on the cyclic behavior of NiAl(Zr) alloys. For example, the fatigue life of binary NiAl is superior to most structural materials at 1000 K compared on a plastic strain range basis due to its high ductility (Ref 20). Therefore, Zr would be expected to reduce this advantage since the ductility of Zr-doped NiAl would be much lower. Conversely, the fatigue life of NiAl is inferior to superalloys on a stress range basis because of its low flow stress. Zirconium might be beneficial in this regard. In addition, fatigue failure of binary NiAl was attributed to an environmentally assisted fatigue damage mechanism that was aggravated by extensive grain boundary void formation due to creep cavitation (Ref 20, 21). Since optimum levels of Zr are beneficial to both the environ-

B.A. Lerch, R.D. Noebe, and **K.B.S. Rao,** NASA Lewis Research Center, Cleveland, OH 44135.

mental resistance and creep resistance of NiAl, it should also be good for low-cycle fatigue (LCF) resistance. However, the final impact of these competing effects on the cyclic deformation behavior of NiAl are too complicated to predict. Therefore, to further understand the role of microalloying additions on the behavior of NiAl, the 1000 K LCF behavior of a NiAl(0.1Zr) alloy prepared by extrusion and HIP consolidation of prealloyed intermetallic powders was investigated. The results are compared to those of similarly processed binary NiAl, and differences in the LCF behavior are explained by the basic differences in the deformation and fracture behavior of the Zr-doped and undoped NiAl.

2. Materials and Experimental Procedures

Vacuum atomized –100/+325 mesh prealloyed powders of stoichiometric NiAl (Heat P2098) and NiAl(0.1Zr) (Heat P1187) were obtained from Homogeneous Metals Inc., Clayville, NY. The chemical compositions of the prealloyed powders are given in Table 1. The Ni, Al, and Zr compositions were determined by inductively coupled plasma (ICP) spectrometry, and interstitial contents were determined by combustion analysis. All chemical analyses were performed at NASA Lewis Research Center.

The nickel aluminide powders were placed in mild steel extrusion cans that were evacuated and sealed air tight. The binary NiAl powder was extruded at 1400 K to an area reduction ratio of 12:1. The stronger Zr-doped alloy was extruded at 1500 K to an area reduction ratio of 12:1. The Zr-doped powder was also consolidated by HIP. The powder was packed in two 304 stainless steel cans approximately 96 mm in diameter by 150 mm long. The cans were evacuated and hot-isostatically pressed at 1533 K and 241 MPa for 5 h. A HIP consolidated binary NiAl alloy processed under identical conditions was previously studied (Ref 20-21). Transmission electron microscopy and additional fractography has since been performed on this binary NiAl alloy, and the results are also reported in this paper.

Cylindrical, dog bone-shaped fatigue samples, 13 mm diameter by 114 mm length, were ground from electrodischarge machined blanks removed from the HIP compacts or directly from the extruded rods. The reduced gage section (22×6.5 mm) of each specimen was electropolished prior to LCF testing in a solution of 90% methanol-10% perchloric acid from 20 to 25 V, 1 A, and 208 K. Fully reversed total axial strain-controlled LCF tests were conducted at 1000 ± 5 K in air, in a servohydraulic system equipped with induction heating. The specimens were gripped by 13 mm-diameter collets inserted into water-cooled, hydraulically actuated grips. Strain was measured using a 13 mm gage length, clip-on, water-cooled extensometer, with alumina probes to allow testing at elevated temperatures. Since room temperature notch sensitivity and brittleness of these intermetallics precluded welding of thermocouples onto the test specimens, temperature was measured and controlled by an infrared pyrometer. A constant total strain rate of 10^{-3}/s and a triangular strain-time waveform was employed for the tests conducted over a strain range from 0.2 to 1.2%.

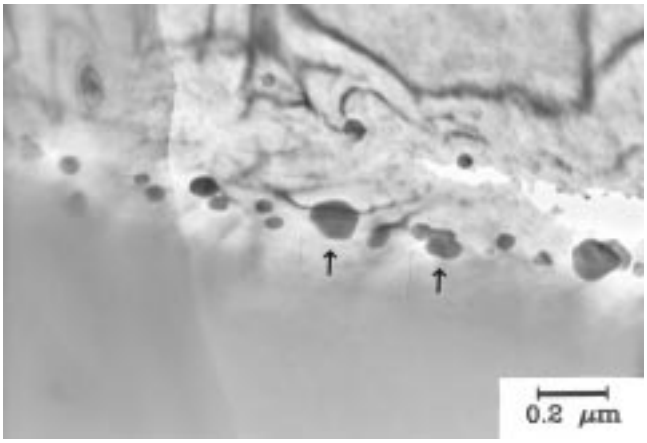

Fig. 1 TEM micrographs showing alumina particles (arrows) in the HIP binary NiAl alloy

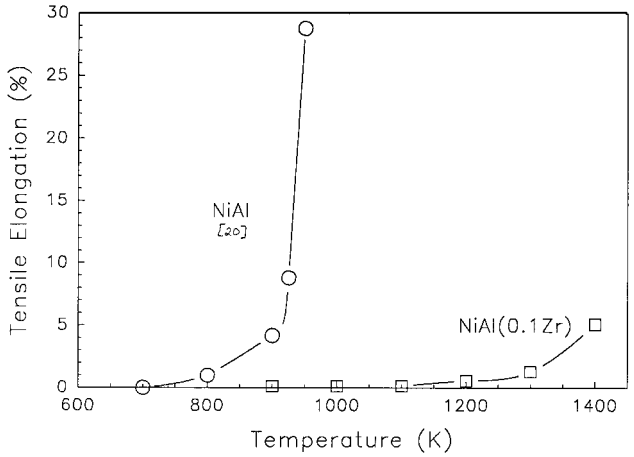

Fig. 2 Tensile ductility of HIP powder processed NiAl and NiAl(Zr) as a function of temperature at an engineering strain rate of 1×10^{-3}/s

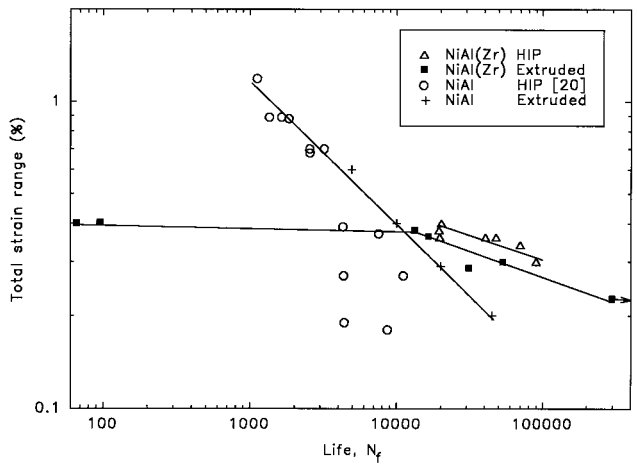

Fig. 3 Total strain-life plots for binary NiAl and NiAl(Zr) processed by extrusion and HIP consolidation of prealloyed powders. The arrow indicates a runout.

Since the brittle-to-ductile transition temperature of the HIP NiAl(Zr) alloy was unknown, additional uniaxial tensile testing was performed on cylindrical buttonhead specimens with a typical gage diameter of 3.2 mm and gage length of 30 mm. Tensile tests were performed between 900 and 1400 K under displacement control and at an initial strain rate of 1.4×10^{-3}/s. A resistance furnace was used for heating, and the temperature gradient along the gage section of the tensile sample was less than ±2 K at all temperatures. In addition, the larger, induction heated, fatigue samples of all four materials were also deformed monotonically at 1000 K, and the tensile data were reported in Table 2. There was excellent agreement between tensile properties determined by the two test techniques.

Examination of the fatigue fracture surfaces was carried out using a scanning electron microscope (SEM). Specimens for transmission electron microscopy (TEM) observation were prepared by electrochemical polishing of thin slices cut from the gage portions of LCF tested specimens. Samples were prepared in a twin-jet polisher using a solution of 70% ethanol, 14% distilled water, 10% butyl cellusolve, and 6% perchloric acid cooled to 263 K. An applied potential of 20 to 25 V with a corresponding current of 10 to 15 mA produced electron transparent foils. TEM samples were examined in a transmission electron microscope operating at 120 kV.

3. Results

All of the HIP and extruded alloys were fully dense and consisted of equiaxed grains. Table 1 provides the average linear intercept grain size for the various nickel aluminide materials. Zirconium doping resulted in a finer average grain size than the binary NiAl processed under identical HIP conditions (Table 1). This is consistent with previous observations (Ref 17) that Zr additions to NiAl retard grain growth during processing. In addition, both extruded alloys exhibited much smaller grain sizes than their respective HIP counterparts due to the much shorter time at the processing temperature. The HIP binary and ternary alloys possessed very fine alumina particles along some grain boundaries (Fig. 1). These are prior particle boundaries that form by breakup, spheroidization, and eventual coarsening of the thin oxide film that covers the as-received powder particles (Ref 17). During extrusion, the powder particles see significantly greater deformation, and therefore, the oxide particles that would make up the prior particle boundaries are more uniformly distributed in the material. Based on the oxygen content of the alloys as shown in Table 1, there is <0.1 vol% oxide present in any of these materials generally distributed along the prior particle boundaries. No other second phase particles were observed in either the binary or Zr-doped alloy. Therefore, for all practical purposes, these powder metallurgy alloys essentially consist of single phase B2-NiAl.

The 1000 K monotonic tensile properties for the four NiAl materials are reported in Table 2. The NiAl(Zr) materials were significantly stronger but exhibited much less tensile ductility than the binary NiAl alloys. Since there were no previous values for the BDTT of HIP NiAl(Zr), additional tensile testing was performed. The tensile ductility for the HIP NiAl(Zr) as a function of temperature is shown in Fig. 2 and compared to the HIP NiAl from Ref 20. The HIP NiAl(Zr) has a tensile ductility of 1% or less below 1300 K and exhibits approximately 5% tensile ductility at 1400 K. Based on the shape of the HIP NiAl ductility versus temperature curve, it can be expected that the BDTT for the HIP NiAl(Zr) is just above 1400 K. These results along with the other BDTTs listed in Table 2 indicate that the BDTT for NiAl(Zr) is approximately 500 K higher than for comparably processed binary NiAl. It is also evident that the fatigue testing temperature of 1000 K is above the BDTT for the binary NiAl materials but is significantly below that of the NiAl(Zr), regardless of processing technique.

The influence of the Zr addition and the effects of processing route on the LCF life of NiAl are demonstrated in Fig. 3. The HIP NiAl(Zr) displayed a marginally higher fatigue resistance than the extruded NiAl(Zr). Zirconium additions were beneficial for the total strain fatigue resistance at strain ranges <0.4%. At strain ranges >0.4%, the binary NiAl materials had

Table 1 Description of NiAl alloys

Alloy	Consolidation method	Grain size, μm	Alloy composition, at.%					
			Ni	Al	Zr	O	C	N
NiAl (Heat P2098)	Extrusion	12 ± 3	50.2 ± 0.2	49.7 ± 0.2	…	0.025	0.017	0.0009
NiAl (Heat P1418)(a)	HIP	70 ± 14	50.5 ± 0.2	49.5 ± 0.2	…	0.028	0.014	0.0006
NiAl(Zr) (Heat P1187)	Extrusion	23 ± 4	49.7 ± 0.2	50.3 ± 0.2	0.094	0.032	0.014	0.0018
	HIP	53		50.3 ± 0.2	0.094	0.032	0.014	0.0018

(a) Alloy studied in Ref 20

Table 2 1000 K tensile properties and BDTT for NiAl and NiAl(Zr) alloys

Alloy	Processing conditions	Elastic modulus, GPa	0.2% Yield stress, MPa	UTS, MPa	Failure strain, %	BDTT	
						K	Ref
NiAl	Extruded	126	80	…	>25	620-670	18
NiAl	HIP	160	75	…	>25	900	20
NiAl(Zr)	Extruded	200	320	328	0.3	1120	6, 18
NiAl(Zr)	HIP	160	360	370	0.4	>1400	This study

BDTT is brittle-to-ductile transition temperature based on a strain rate of 1×10^{-3}/s.

better fatigue resistance. However, the extruded NiAl intermetallic had a better fatigue resistance at the low strain ranges compared to the HIP consolidated powder because the HIP binary NiAl alloy exhibited a break in the slope of the total strain range versus life curves.

Typical stress response curves for the binary and Zr-doped NiAl during cyclic loading are shown in Fig. 4 for total strain ranges of nominally 0.4%. These curves represent the locus of peak tensile stress amplitudes with each successive cycle. It is immediately apparent that alloying NiAl with zirconium resulted in much higher response stresses. The NiAl(Zr) alloy in the HIP and extruded conditions displayed similar stress responses. The Zr-doped materials exhibited a very short period of cyclic hardening and attained the maximum stress in the early stages of cyclic life. Beyond the maximum stress value, a gradual softening took place before a regime of nearly stable stress response commenced. This stable stress response regime was found to extend with decreasing strain range. The binary alloy in the HIP condition displayed larger response stresses than the extruded binary NiAl, and both materials displayed a slight softening throughout the life. However, the amount of change in the stress response for either the NiAl(Zr) or NiAl was extremely small (<40 MPa) and for most engineering purposes can be neglected.

Table 3 Cyclic stress-strain values
$\Delta\sigma/2 = K'(\Delta\varepsilon_p/2)^{n'}$

Alloy	Processing conditions	K', MPa	n'
NiAl	HIP	256	0.11
NiAl	Extruded	90	0.07
NiAl(Zr)	HIP, extruded	1346	0.18

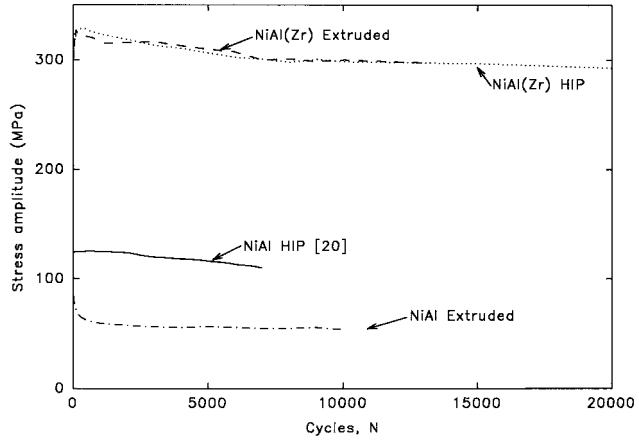

Fig. 4 Cyclic stress response curves for NiAl and NiAl(Zr) tested at a total strain range of nominally 0.4%

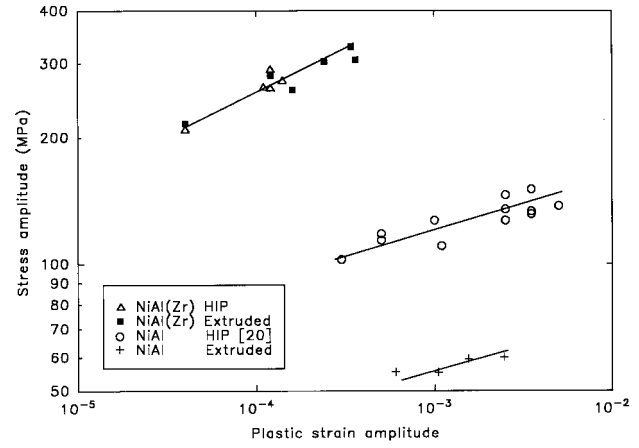

Fig. 5 Cyclic stress-strain curves for binary and Zr-doped NiAl

The cyclic stress-strain curves at 1000 K for each material investigated are given in Fig. 5 in the form of a log-log plot of the half-life tensile stress amplitude ($\Delta\sigma/2$) versus the corresponding plastic strain amplitude ($\Delta\varepsilon_p/2$). It was observed that the cyclic stress-strain relationship can be represented by a power law of the form $\Delta\sigma/2 = K' (\Delta\varepsilon_p/2)^{n'}$, where K' and n' are the cyclic strength coefficient and cyclic strain hardening exponent, respectively. The values of K' and n', obtained from least squares analyses of the data are included in Table 3. The cyclic stress-strain curves for the extruded and HIP NiAl(Zr) could be represented by a single line. Figure 5 and Table 3 clearly show that the Zr-doped alloy has a higher cyclic strength and exhibits a higher cyclic strain hardening exponent compared to the binary NiAl. The binary alloy displayed a significantly higher cyclic strength, but only a marginally higher cyclic strain hardening exponent in the HIP condition than in the extruded condition.

The extruded NiAl(Zr) exhibited a brittle mixed mode (transgranular cleavage plus intergranular) failure appearance at a strain range of 0.4% with no evidence of stable crack growth (Fig. 6a). For strain ranges ≤0.38%, failure initiated through slow, stable, intergranular crack growth (Fig. 6b), with final tensile overload failure occurring by mixed mode fracture. Longitudinal sections of the failed specimens revealed very few secondary cracks emanating from the surface in the gage section, but the ones observed also indicated that the nature of crack initiation and propagation was intergranular at strain ranges less than 0.38%. Also, a small number of grain boundaries exhibited cavities (Fig. 6c). The fractographic features and the damage behavior of HIP NiAl(Zr) at various strain ranges were similar to those presented above for the extruded NiAl(Zr).

In the HIP NiAl, at all the strain ranges, crack initiation and initial propagation remained intergranular. Final crack propagation was due to tensile overload, and this occurred primarily by transgranular cleavage. Approximately 20 to 40% of the fracture surface of the binary NiAl was due to stable fatigue crack growth, which could be easily identified by a dark ring on the sample surface as a result of oxidation (Fig. 7a). The oxidation damage was more extensive at strain ranges ≤0.5%. In addition, at low strain ranges, a high percentage of the grain boundaries contained voids (Fig. 7b). However, the grain boundaries that cavitated did not show any particular angular relationship with respect to the applied stress axis. The extruded NiAl also exhibited stable intergranular crack growth at all strain ranges with intergranular cracking extending to approximately 80% of the fracture surface. Characterization of

the gage surface of fatigue tested samples showed brittle decohesion of the grain boundaries (Fig. 8a). The number of cracked grain boundaries was extremely high, and propagation occurred by interlinkage of these intergranular cracks. Operation of this process has led to an intergranular fracture surface as illustrated in Fig. 8(b).

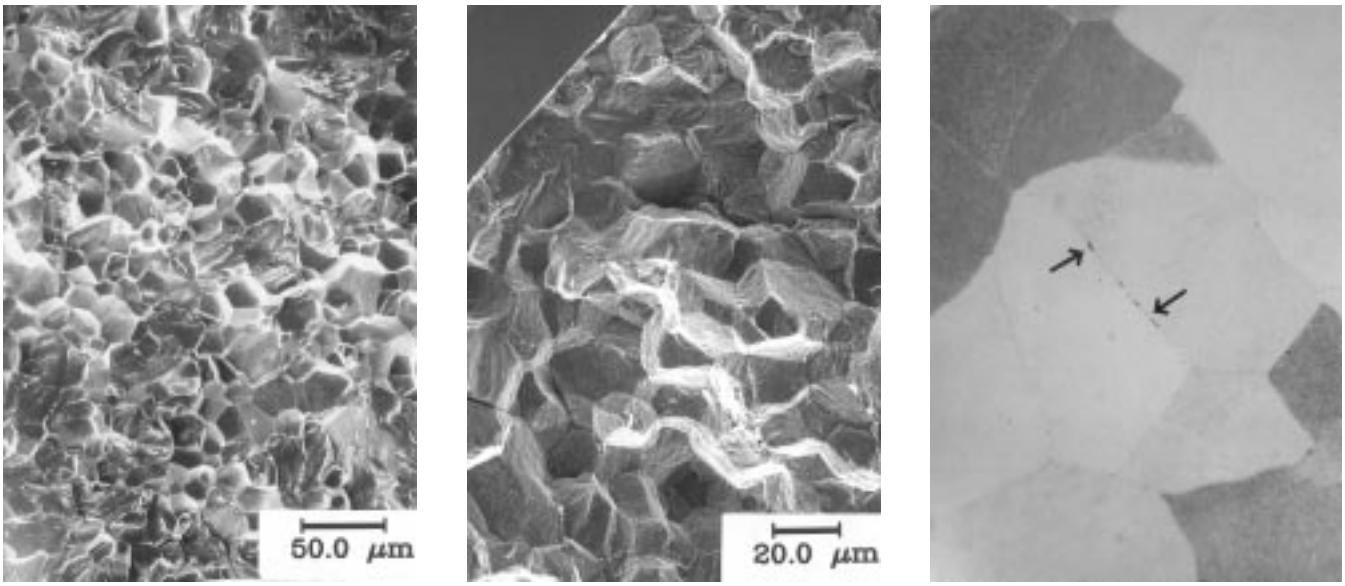

(a) **(b)** **(c)**

Fig. 6 Fatigue damage in extruded NiAl(Zr). (a) Mixed mode failure consisting of transgranular cleavage and intergranular cracking at a total strain range of 0.40%. (b) Intergranular crack initiation of a specimen tested at a total strain range of 0.29%. (c) Intergranular cavities in a longitudinally sectioned sample tested at a total strain range of 0.36%

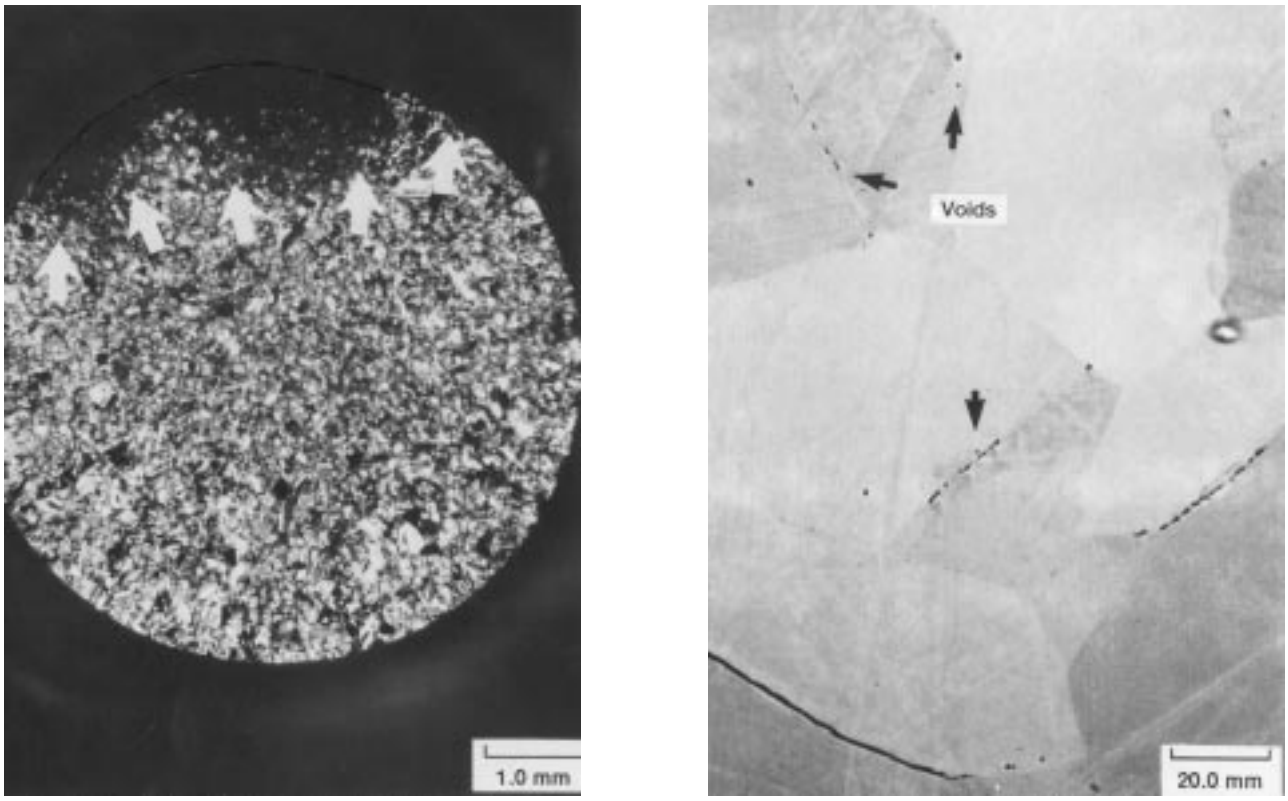

(a) **(b)**

Fig. 7 (a) Fracture surface of a HIP NiAl specimen tested at a strain range of 0.88%. Arrows indicate extent of slow and stable intergranular crack growth. (b) Intergranular cavitation on numerous grain boundaries in a specimen tested at 0.27%

Transmission electron microscopy analysis revealed some interesting results concerning the cyclic deformation behavior of NiAl(Zr). The ternary alloy consisted of a high but uniformly distributed density of dislocations throughout the grain interiors along with a significant number of very fine dislocation loops (Fig. 9a). The most interesting feature of the Zr-doped alloy, however, was the presence of dislocation-free zones along most of the grain boundaries (Fig. 9b). The grain boundaries also contained very fine precipitates, which formed during LCF testing (Fig. 9c). These particles are probably precipitates of the Heusler phase Ni_2AlZr (Ref 19). A loss in creep strength after aging of NiAl(Zr) alloys has also been attributed to the precipitation of the Heusler phase in what were originally single-phase solid-solution alloys (Ref 22).

In contrast to the deformation behavior of the ternary alloy, the extruded binary NiAl exhibited well-developed subcells with the interior regions of the cells remaining relatively free from dislocations at low strain ranges (Fig. 10a). At high strain ranges, the dislocations were more homogeneously distributed (Fig. 10b). The deformation behavior of the HIP binary alloy at all the strain ranges was characterized by a cell-type network (Fig. 11) with a very high density of dislocation loops in the cell walls.

4. Discussion

In the case of the HIP binary NiAl, the samples cycled at low strain ranges exhibited much shorter lives than would be ex-

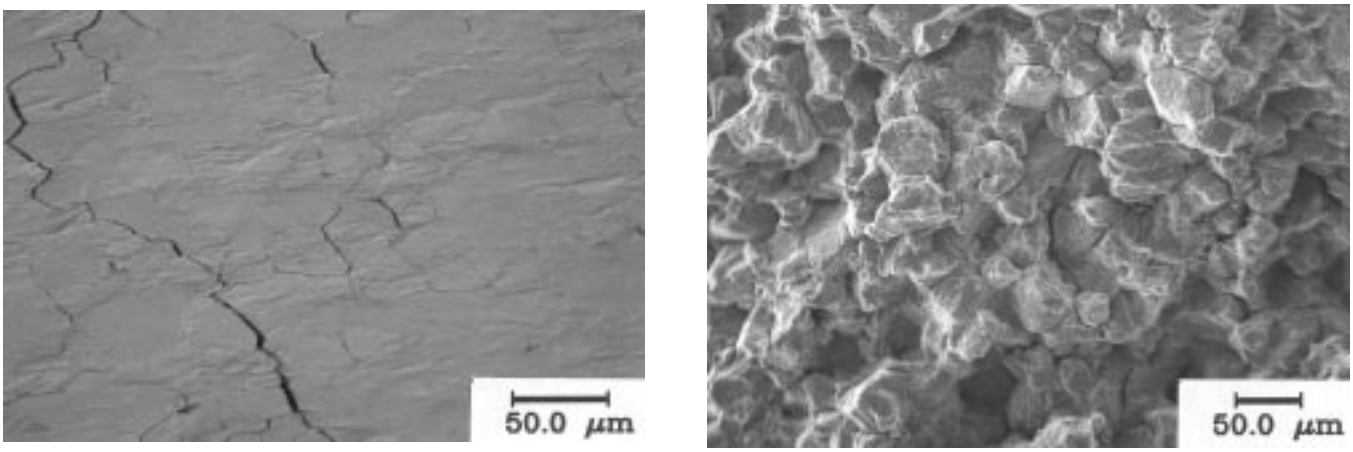

(a) **(b)**

Fig. 8 SEM micrographs of an extruded NiAl specimen tested at a strain range of 0.2% showing (a) brittle intergranular decohesion on the gage surface and (b) severe intergranular fracture

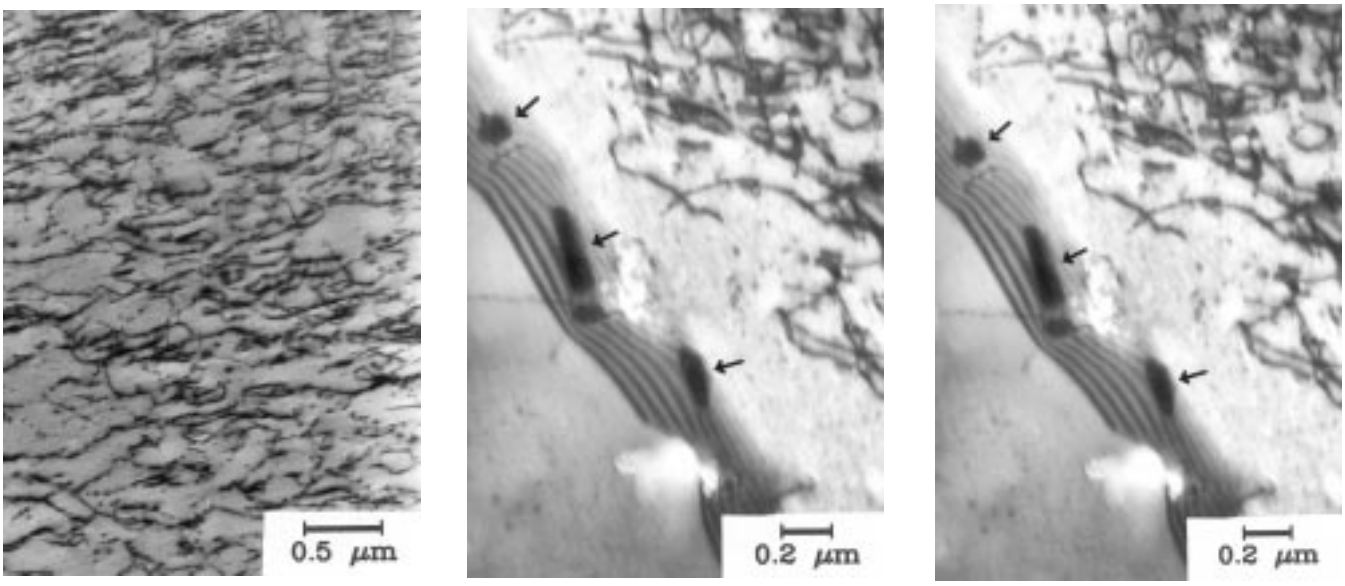

(a) **(b)** **(c)**

Fig. 9 Deformation substructures in extruded NiAl(Zr) tested at a total strain range of 0.30%. (a) Typical dislocation distribution within grain interiors. (b) Dislocation free zones along a grain boundary (arrows). (c) Fine intergranular precipitates (arrows) formed during LCF testing

pected by extrapolation from the high strain range portion of the total strain-life plot (Fig. 3). Such nonideal strain-life behavior resulting in a discontinuity has also been observed in several nickel-base superalloys (Ref 23-26), aluminum alloys (Ref 27, 28), and dual-phase steels (Ref 29). The bilinear nature of strain-life plots has been correlated with (a) the differences in crack initiation and propagation modes at low and high strain ranges (Fig. 23), (b) the changes in deformation mechanisms (Ref 24, 25, 30), and (c) the synergistic interaction between fatigue and oxidation (Ref 31).

The discontinuity in the strain-life curve of the HIP NiAl occurred as a consequence of the operation of different damage mechanisms in the high and low life regimes. In the low life regime (high strain ranges), there was no major interaction between fatigue and other time dependent processes, that is, oxidation or creep, and the life was dictated predominantly by fatigue crack initiation and growth. In the long life regime (low strain ranges), creep and environmentally activated damage micromechanisms were combined with fatigue damage and led to a drastic reduction in life. All the creep cavities on grain boundaries of the HIP binary alloy were rounded in shape (r-type) with no evidence for triple point wedge cracking. The creep cavities in the HIP condition are believed to be associated with the alumina particles that were present on the grain boundaries. It is well established that secondary phases on the grain boundary can provide suitable nucleation sites for intergranular cavities (Ref 32, 33). These isolated cavities grow by the diffusional transport of vacancies or by the deformation of matrix material and, therefore, do not necessarily require grain boundary sliding (Ref 32-34). Few alumina particles were located at the grain boundaries in the extruded NiAl, which reduced the amount of creep cavities in this material, and therefore the life of the extruded binary NiAl at low strain ranges was not affected like the HIP NiAl and did not display the bilinear fatigue life behavior.

Attributing the bilinear life behavior of the HIP NiAl to pore formation is consistent with previous observations on this alloy presented in Ref 20 and 21. When the HIP alloy is tested in vac-

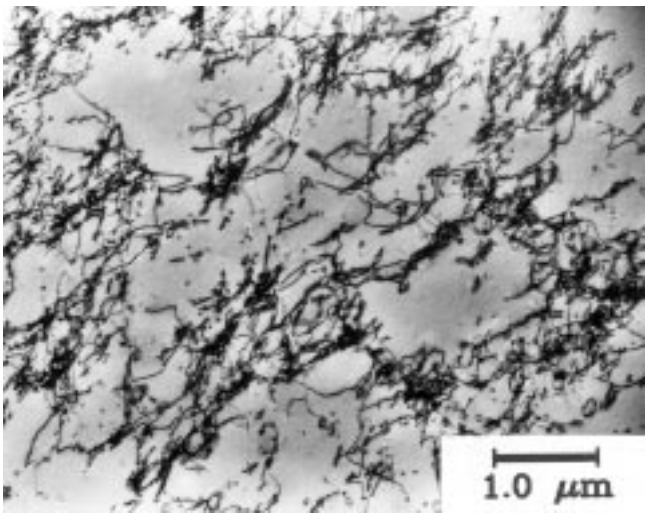

(a)

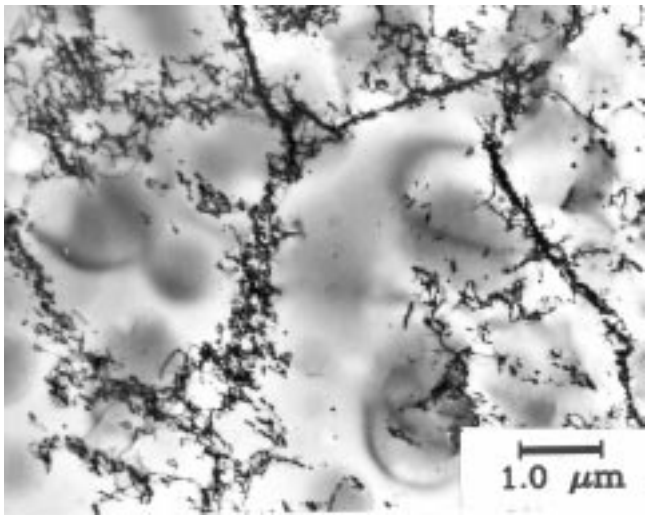

(b)

Fig. 10 Deformation substructures in extruded binary NiAl (a) at a strain range of 0.30% and (b) at a strain range of 0.60%

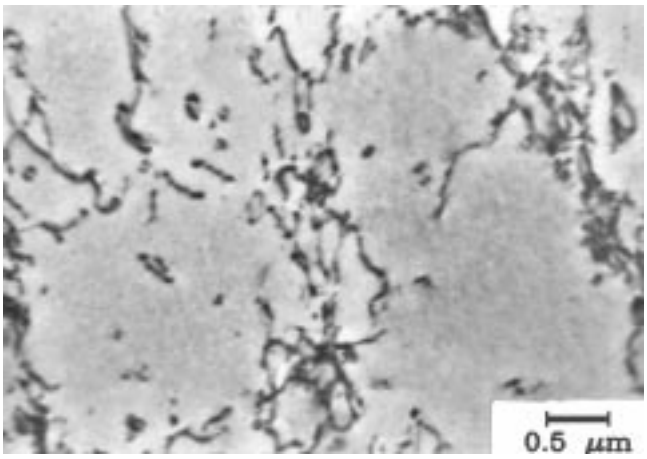

Fig. 11 Cell-type structure in a HIP binary NiAl specimen tested at a strain range of 0.30%

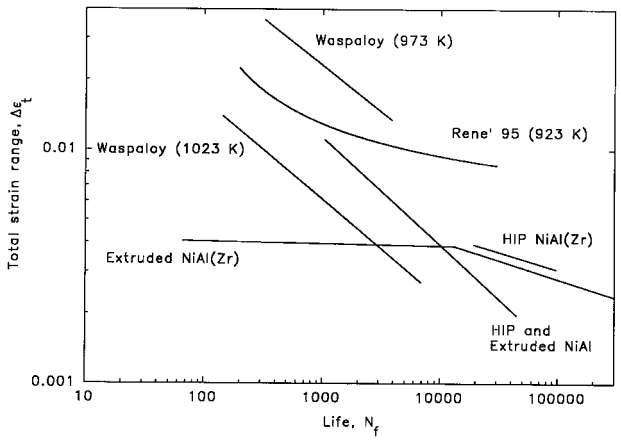

Fig. 12 Total strain range-life curves for various superalloys and nickel aluminides

uum, there is a three-fold increase in fatigue life, but the material still displays a bilinear fatigue life behavior. Therefore, reducing the environmental problem affected the life but did not alter the bilinear strain life behavior of the material. Thus, pore formation at the grain boundaries, which is most prominent in the HIP NiAl alloy, must be responsible for the loss in fatigue life at lower strain ranges.

The break in the strain-life curve (Fig. 3) of the extruded NiAl(Zr) is due to a completely different mechanism from that which has been proposed for the HIP NiAl. The two stages in the strain-life plot of the extruded NiAl(Zr) resulted from a sudden loss of life on raising the total strain range from 0.38% (13,270 cycles) to 0.4% (66 cycles). This transition has been found to correlate with a change in the fracture mode from slow and stable intergranular crack growth at the lower strain ranges to a completely brittle cleavage fracture at the upper strain ranges. During cyclic deformation at 0.4%, a peak tensile stress was developed in less than 100 cycles (328 MPa), which equaled the monotonic tensile cleavage fracture stress of the Zr-doped alloy at 1000 K (Table 2), enabling brittle overload fracture to occur. At a total strain range of 0.38%, the maximum cyclic tensile stress attained during cycling (306 MPa) was much less than the cleavage fracture stress, and therefore, the material was able to accumulate a large number of cycles before failure took place by slow and stable crack growth. The LCF tests on the HIP NiAl(Zr) were not conducted at strain ranges higher than 0.4% due to the lack of samples. However, tests at higher strain ranges would be expected to follow the behavior exhibited by the extruded alloy. The brittle fracture of the Zr-doped alloy imposes a limitation on the maximum strain range at which the alloy can be used.

The Zr-doped NiAl in both processing conditions showed better fatigue resistance than the binary alloy below a strain range of 0.38%. This increase in the LCF life of the less ductile NiAl(Zr) alloy can be rationalized by two factors. The first relates to the segregation of Zr to the grain boundaries. Compositional analysis of extruded samples by auger electron spectroscopy showed an average concentration of 5 to 6 at.% Zr at the grain boundaries compared to 0.1 at.% Zr in the bulk of the material (Ref 17). The tendency for grain-boundary cavity formation was reduced in the Zr-doped alloy, regardless of processing technique. Both the number of grain boundaries that have been cavitated and the number of cavities on the boundaries were much smaller compared to those in comparably processed binary NiAl. However, due to the high density of intergranular cracks observed on the gage surface of the specimens, there was no overwhelming evidence to suggest that the Zr addition helped retard oxidation damage during crack initiation. However, it is possible that by reducing the cavitation at the boundaries and by increasing the grain boundary cohesion, Zr could reduce the rate of fracture propagation along the grain boundaries. This would in part explain the longer lives of the Zr-doped samples even though the response stresses were several times larger than those of binary NiAl.

The second factor that could explain the improved fatigue resistance of the Zr-doped alloy over the undoped NiAl is its basic capacity to resist the applied strain range on the basis of its high strength. Fatigue life is generally governed by the ductility of the material at high strains and by the strength of the material at low strains. Since the strength of the material was increased by the addition of Zr, the plastic strain component generated at a given total strain range was significantly smaller compared to that of the binary NiAl. Therefore, at low strain ranges, the Zr-doped alloys resisted the imposed total strain on the basis of its strength, leading to an improvement in fatigue life. The slight improvement in the HIP NiAl(Zr) over the extruded NiAl(Zr) can be explained similarly. An analysis of the LCF results revealed that the plastic strains accumulated in the HIP NiAl(Zr) were ≈3 times less than that of the extruded alloy. Typically, at an applied total strain range of 0.3%, the HIP alloy developed a plastic strain range of 0.008% compared to 0.024% for the extruded material. This observation suggests that in the HIP material, tensile ductility exhaustion occurred at a much slower rate compared to the extruded alloy, leading to larger number of cycles to failure in the HIP NiAl(Zr).

The cyclic strain hardening exponent, n', generally serves as an indicator of the deformation behavior and as a guide for estimating LCF resistance. In the current study, n' was proportional to the fatigue life exhibited by the binary and Zr-doped NiAl; the NiAl(Zr) exhibited a higher n' value and a higher life. The correlation between high n' and improved fatigue resistance agrees with the analysis of Feltner and Beardmore (Ref 35) and Rao (Ref 36), who suggested that the larger values of n' correspond to an increased resistance to cyclic strains. In NiAl(Zr), the more homogeneous deformation within the grains, the mutual interactions between dislocations, and the interactions of dislocations with Zr atoms seems to cause higher cyclic stresses and a higher n'. Zirconium additions have been reported to cause a dramatic increase in the lattice resistance to dislocation motion and are very effective in pinning dislocations and preventing their motion until much higher temperatures are reached (Ref 6, 16, 18), thus resulting in a much higher BDTT. The lower n' of the binary NiAl, in general, coincides with the occurrence of thermal recovery, which is characterized by the formation of cells and subgrains. Rearrangement of dislocations into cells and subgrains is believed to be the cause for the softer behavior in the binary NiAl. This behavior is a direct consequence of testing significantly above the BDTT of the binary alloy. In the case of the NiAl(Zr), the test temperature is below its BDTT, and thermal processes are minimal, thus leading to harder behavior.

In the case of binary NiAl, the HIP alloy displayed comparatively larger cyclic strength than the extruded alloy. This is due to the more recovered structure exhibited by the extruded material shown in Fig. 10 compared to the HIP NiAl shown in Fig. 11. These structures are again commensurate with the relationship between the test temperature (1000 K) and the BDTT of each material as listed in Table 2. The difference between the test temperature and the BDTT is greater for the extruded NiAl, implying that this material should exhibit more creep recovery, as the microstructure has indeed indicated.

Figure 12 illustrates fatigue life of NiAl and Zr-doped alloys that have been compared to two superalloys at a nominal temperature of 1000 K. The two polycrystalline nickel-base alloys used for comparison were Waspaloy (Ref 37), and René 95 (Ref 37). Both NiAl materials fall mostly within the range of superalloy data. However, the Zr-doped NiAl is inferior to the

superalloys at high total strain ranges due to the rapid attainment of the cleavage fracture stress.

5. Summary and Conclusions

Small amounts of Zr had a large effect on the fatigue behavior of NiAl at 1000 K. Zirconium raised the BDTT of the alloy above the test temperature. This resulted in a higher monotonic and cyclic strength, but with much less ductility for the Zr-doped material. When both strength and ductility were taken into account by testing under a total strain range, the Zr-doped materials showed improved lives over binary NiAl. At a total strain range of 0.4%, however, the Zr-doped material reached its monotonic cleavage fracture stress very early in the life and failed at very short fatigue lives. Therefore, above a total strain range of 0.4%, the binary alloy had superior lives. Both NiAl and NiAl(Zr) had similar fatigue lives to selected superalloys nominally tested at 1000 K.

Acknowledgments

The authors wish to thank Dr. G.R. Halford for many stimulating discussions and encouragement. K. Bhanu Sankara Rao wishes to acknowledge the National Research Council, Washington, D.C., for granting the fellowship. The diligent efforts of Mr. Ralph Corner in the fatigue laboratory are gratefully acknowledged.

References

1. D.B. Miracle, *Acta Metall. Mater.*, Vol 39, 1993, p 649
2. R.D. Noebe, R.R. Bowman, and M.V. Nathal, *Physical Metallurgy and Processing of Intermetallic Compounds*, N.S. Stoloff and V.K. Sikka, Ed., Chapman & Hall, 1996, p 212-296
3. R. Darolia, *JOM*, Vol 43 (No. 3), 1991, p 44
4. C.T. Liu and K.S. Kumar, *JOM*, Vol 45 (No. 5), 1993, p 38
5. R. Darolia, D. Lahrman, and R.D. Field, *Scr. Metall. Mater.*, Vol 26, 1992, p 1007
6. R.D. Noebe and M.K. Behbehani, *Scr. Metall. Mater.*, Vol 27, 1992, p 1795
7. E.P. George and C.T. Liu, *J. Mater. Res.*, Vol 5, 1990, p 754
8. R.D. Noebe, R.R. Bowman, and M.V. Nathal, *Int. Mater. Rev.*, Vol 38, 1993, p 193
9. J.D. Cotton, R.D. Noebe, and M.J. Kaufman, *Intermetallics*, Vol 1, 1993, p 3
10. P.H. Kitabjian, A. Garg, R.D. Noebe, and W.D. Nix, *Creep and Fracture of Engineering Materials and Structures*, J.C. Earthman and F.A. Mohamed, Ed., The Minerals, Metals & Materials Society, 1997, p 667-676
11. I.E. Locci, R. Dickerson, R.R. Bowman, J.D. Whittenberger, M.V. Nathal, and R. Darolia, *High Temperature Ordered Intermetallic Alloys V*, I. Baker et al., Ed., Vol 288, Materials Research Society, Pittsburgh, PA, 1993, p 685-690
12. R. Darolia and W.S. Walston, *Structural Intermetallics 1997*, M.V. Nathal et al., Ed., The Minerals, Metals & Materials Society, 1997, p 585-594
13. C.A. Barrett, *Oxid. Met.*, Vol 30, 1988, p 361
14. J. Doychak, J.L. Smialek, and C.A. Barrett, *Oxidation of High-Temperature Intermetallics*, T. Grobstein and J. Doychak, Ed., The Minerals, Metals & Materials Society, 1989, p 41-55
15. S.V. Raj, R.D. Noebe, and R.R. Bowman, *Scr. Metall.*,Vol 23, 1989, p 2049
16. R.R. Bowman, R.D. Noebe, S.V. Raj, and I.E. Locci, *Metall. Trans. A*, Vol 23, 1992, p 1493
17. M.V. Zeller, R.D. Noebe, and I.E. Locci, in *HITEMP Review—1990*, NASA CP-10051, 1990, p 21-1 to 21-17
18. R.D. Noebe, NASA TM-106534, April 1994
19. J.D. Whittenberger and R.D. Noebe, *Metall. Mater. Trans. A*, Vol 27, 1995, p 2628
20. B.A. Lerch and R.D. Noebe, *Metall. Mater. Trans. A*, Vol 25, 1994, p 309
21. K.B.S. Rao, B.A. Lerch, and R.D. Noebe, *Fatigue and Fracture of Ordered Intermetallic Alloys II*, W. Soboyejo and T.S. Srivatsan, Ed., The Minerals, Metals & Materials Society, 1995, p 245-271
22. J.D. Whittenberger and R.D. Noebe, *Mater. Lett.*, Vol 27, 1996, p 281
23. M. Valsan, K.B.S. Rao, and S.L. Mannan, *Trans. Indian Inst. Met.*, Vol 42s, 1989, p s203
24. M. Valsan, K.B.S. Rao, M. Vijayalakshmi, S.L. Mannan, and D.H. Shastry, *Metall. Trans. A*, Vol 23, 1992, p 1751
25. B.A. Lerch and V. Gerold, *Acta Metall.*, Vol 33, 1985, p 1709
26. M. Clavel, C. Levaillant, and A. Pineau, *Proc. Conf. on Creep-Fatigue-Environment Interactions*, R.M. Pelluox and N.S. Stollof, Ed., The Metallurgical Society of AIME, 1980, p 24-44
27. T.M. Sanders, Jr. and E.A. Starke, Jr., *Metall. Trans. A*, Vol 7, 1976, p 1007
28. R.E. Sanders, Jr. and E.A. Starke, Jr., *Mater. Sci. Eng.*,Vol 28, 1976, p 53
29. S.R. Mediratta, V. Ramaswamy, and P. Rama Rao, *Scr. Metall.*, Vol 20, 1986, p 555
30. C.H.D. Arbuthnot, in *Proc. 4th European Conf. on Fracture*, Engineering Materials Advisory Services, Ltd., Warley, England, 1982, p 407-413
31. L.F. Coffin, Jr., *J. Mater. Sci.*, Vol 6, 1971, p 388
32. K.B.S. Rao, H.P. Meurer, and H. Schuster, *J. Mat. Sci.*, Vol A104, 1988, p 37
33. P. Rodriguez and K.B.S. Rao, *Prog. Mater. Sci.*, Vol 37, 1993, p 403
34. R. Raj, *Acta Metall.*, Vol 26, 1976, p 1007
35. C.E. Feltner and P. Beardmore, ASTM STP 467, Vol 77, 1970
36. K.B.S. Rao, Influence of *Metallurgical Variables on Low Cycle Fatigue Behavior of Type 304 Stainless Steel*, Ph.D. thesis, Univ. of Madras and IGCAR-Kalpakkam, India, Jan 1989
37. *Characterization of Low Cycle High Temperature Fatigue by the Strain Range Partitioning Method*, AGARD CP-243, 1978